Editors' Suggestion

Limits on Supernova-Associated ^{60}Fe/^{26}Al Nucleosynthesis Ratios from Accelerator Mass Spectrometry Measurements of Deep-Sea Sediments

Jenny Feige,[1,2,*] Anton Wallner,[3] Randolf Altmeyer,[4] L. Keith Fifield,[3] Robin Golser,[2] Silke Merchel,[5] Georg Rugel,[5] Peter Steier,[2] Stephen G. Tims,[3] and Stephan R. Winkler[2,6]

[1]*Technische Universität Berlin, Department of Astronomy and Astrophysics, Hardenbergstr. 36, 10623 Berlin, Germany*
[2]*University of Vienna, Faculty of Physics-Isotope Research and Nuclear Physics, VERA Laboratory, Währingerstr. 17, 1090 Vienna, Austria*
[3]*The Australian National University, Department of Nuclear Physics, Canberra ACT 2601, Australia*
[4]*Humboldt-Universität zu Berlin, Department of Mathematics, Unter den Linden 6, 10099 Berlin, Germany*
[5]*Helmholtz-Zentrum Dresden-Rossendorf, Helmholtz Institute Freiberg for Resource Technology, Bautzner Landstr. 400, 01328 Dresden, Germany*
[6]*iThemba LABS—Laboratory for Accelerator Based Science, Somerset West 7129, South Africa*

We searched for the presence of ^{26}Al in deep-sea sediments as a signature of supernova influx. Our data show an exponential dependence of ^{26}Al with the sample age that is fully compatible with radioactive decay of terrigenic ^{26}Al. The same set of samples demonstrated a clear supernova ^{60}Fe signal between 1.7 and 3.2 Myr ago. Combining our ^{26}Al data with the recently reported ^{60}Fe data results in a lower limit of $0.18^{+0.15}_{-0.08}$ for the local interstellar ^{60}Fe/^{26}Al isotope ratio. It compares to most of the ratios deduced from nucleosynthesis models and is within the range of the observed average galactic ^{60}Fe/^{26}Al flux ratio of (0.15 ± 0.05).

The radionuclides ^{26}Al ($t_{1/2} = 0.717 \pm 0.017$ Myr [1]) and ^{60}Fe ($t_{1/2} = 2.61 \pm 0.04$ Myr [2–4]) are key isotopes for understanding nucleosynthesis in our Galaxy. Both were present in the early Solar System, as evidenced by an excess of their decay products in meteorites [5,6]. Today, the decay of live ^{26}Al and ^{60}Fe is observed in the interstellar medium (ISM) through their associated characteristic γ-rays [7,8].

Significant amounts (3–10%) of ^{26}Al and ^{60}Fe are freshly synthesized and ejected into the ISM by (super) asymptotic giant branch—(S)AGB—stars in the mass range of $\sim$5–9 $M_\odot$ [9,10]. However, the major fraction is thought to be released by massive stars ($\gtrsim$9 $M_\odot$) that explode as core-collapse supernovae (CCSNe) [11–13]. Electron-capture (EC)SNe ($\sim$7–11 $M_\odot$) produce ^{60}Fe, but negligible ^{26}Al during explosive nucleosynthesis [10,14]. Additionally, stellar winds of Wolf-Rayet (WR) stars with masses > 40 $M_\odot$, which also end their lives as SNe, have been proposed as major sources for the galactic ^{26}Al inventory [15,16], while they are not believed to contribute significant amounts of ^{60}Fe [13,17]. Hence, the observed ISM distribution of ^{26}Al and ^{60}Fe combines a mixture of different stellar sources, with a galactic averaged ^{60}Fe/^{26}Al γ-ray flux ratio of (0.15 ± 0.05) [8].

Freshly produced radionuclides from supernova (SN) explosions can be transported over large interstellar distances. Material ejected from nearby SNe can enter our Solar System and cross Earth's orbit, potentially leaving traces of the ejecta in terrestrial archives [18,19]. Indeed, the radionuclide ^{60}Fe has been identified in terrestrial [20–24] and lunar samples [25]. The detection of SN-associated ^{60}Fe deposited about 2–3 Myr ago provides an opportunity to determine the specific SN-associated ^{26}Al/^{60}Fe ratio, disentangling it from the observed galactic average ratio.

Here, we present for the first time a detailed ^{26}Al time profile and combine this data with the previously measured SN-associated ^{60}Fe data from the same deep-sea sediments [22] to derive the ^{60}Fe/^{26}Al ratio associated with the recent and local SN events. First, we estimate whether SN-associated ^{26}Al is within the detection limit of accelerator mass spectrometry (AMS) using an ^{60}Fe/^{26}Al isotope ratio of 0.5. Furthermore, we compare our derived SN-associated ^{60}Fe/^{26}Al ratio to SN nucleosynthesis models and to the observed galactic averaged ^{60}Fe/^{26}Al γ-ray flux ratio.

We have quantified the ^{26}Al content of a total of 83 samples from four *Eltanin* cores from the Indian Ocean, located $\sim$1000 km south-west of Australia: ELT 45-16, ELT 45-21, ELT 49-53, and ELT 50-02 [26,27]. The cores were recovered in the years 1970 and 1971 from depths of $\sim$4300 m below the sea surface at locations of 35°0.7'S–9° 58'S and 100°02'E–104°56'E. The largest set of samples was taken from ELT 45-21 (28 samples) from depths of 398–697 cm below the ocean floor and from ELT 49-53 (45 samples) from depths of 120–517 cm, collected at 3–17 cm increments with average lengths of $\sim$1 cm [28].

For age determination, preexisting magnetostratigraphic data [29] were combined with radioisotopic dating values using the decay of atmospherically produced (cosmogenic) [10]Be [22]. The resulting sediment accumulation rates were $\sim$3 mm kyr^{-1}. Samples ($\sim$3 g each) from the two largest sets cover the time range of the enhanced [60]Fe signal: ELT 45-21 between 1.8 and 2.6 Myr ago and ELT 49-53 between 1.7 and 3.2 Myr. Additionally, recent (near-surface) samples were studied. The silt and clay dominated [29] sediment samples were leached with a mild acid to extract the authigenic Al fraction and chemically treated using a procedure described elsewhere [28,30,31]. On average, 3 mg of Al_2O_3 was produced from each sample.

Assuming an [60]Fe/[26]Al isotope ratio of 0.5 (e.g., [32]) and the identical transport of [26]Al and [60]Fe, we can estimate the SN-associated [26]Al deposition in terrestrial archives from the [60]Fe signal. Using the decay-corrected concentration of $(5–10) \times 10^4$ atoms g^{-1} of [60]Fe (see Table 1 in Ref. [22], corresponding to an average deposition rate of $\sim$25 atoms cm^{-2} yr^{-1}), we would expect $(1–2) \times 10^5$ [26]Al atoms g^{-1} sediment (or $\sim$50 atoms cm^{-2} yr^{-1}) at the time of deposition. After 2.6 Myr of radioactive decay (corresponding approximately to the SN peak's center) $(0.9–1.7) \times 10^4$ atoms g^{-1} are left.

The only method sensitive enough to measure such low concentrations is AMS. The [26]Al content of the leachate was determined via [26]Al/[27]Al isotope ratio measurements at the AMS facility VERA (Vienna Environmental Research Accelerator) at the University of Vienna, Austria. The amount of stable authigenic [27]Al was measured with inductively coupled plasma mass spectrometry (ICP-MS) at the Helmholtz-Zentrum Dresden-Rossendorf, Germany. On average, each sample leachate contained $(1.86 \pm 0.07) \times 10^{19}$ atoms g^{-1} of [27]Al (see Supplemental Material [33]). This value combined with the estimated SN-associated [26]Al value of $(0.9–1.7) \times 10^4$ atoms g^{-1} results in an isotope [26]Al/[27]Al ratio of $(0.5–1) \times 10^{-15}$, a ratio very close to the detection limit of $\sim$6 $\times 10^{-16}$. With an overall detection efficiency of 2×10^{-4} [34] for [26]Al at VERA, the estimated SN-associated [26]Al influx would result in the detection of 5–10 [26]Al atoms per 3 g sample.

Concurrent natural [26]Al production on Earth makes the detection of any SN-associated [26]Al influx above the terrestrial background challenging. The main production mechanisms of [26]Al in the Earth's atmosphere are spallation reactions via cosmic-ray particles on argon [35]. A mean atmospheric flux of $\sim$1280 [26]Al atoms cm^{-2} yr^{-1} is observed in the Earth's atmosphere, of which about 5% originate from influx of extraterrestrial matter such as meteorites and interplanetary dust [36]. These constantly produced cosmogenic radionuclides reach the deep-sea sediment surfaces on timescales of 100 years [37] and make up our baseline background above which a SN-associated [26]Al signal has to be detected. Postdepositional *in situ* production also

contributes to the terrestrial [26]Al background, albeit at lower yields [38].

The individual samples were measured with AMS for several hours each until fully consumed, resulting in a precision of between 3 and 15%. While the modern surface samples yielded up to 1240 counts of [26]Al atoms in a single 3 g sample, the 3 Myr old samples yielded only $\sim$70 counts. The measured [26]Al/[27]Al ratios, containing the terrigenic and any potential SN-associated [26]Al, were found to exponentially decrease with increasing age [Fig. 1(a)].

In the following, we investigate whether the data show any SN-associated [26]Al influx on top of the baseline influx of [26]Al. We assume a constant production rate for [26]Al that is dominated by cosmogenic atmospheric production neglecting *in situ* production, and no significant SN-associated influx at present time, as demonstrated by the [60]Fe data [22] [Fig. 1(b)]. Five surface samples yielded a modern ratio of [26]Al/[27]Al $= (2.56 \pm 0.08) \times 10^{-13}$, which was used to calculate an exponential function with its error [Fig. 1(a)]. This modern [26]Al/[27]Al surface ratio is in excellent agreement with the decay-corrected average of all samples between 1.7 and

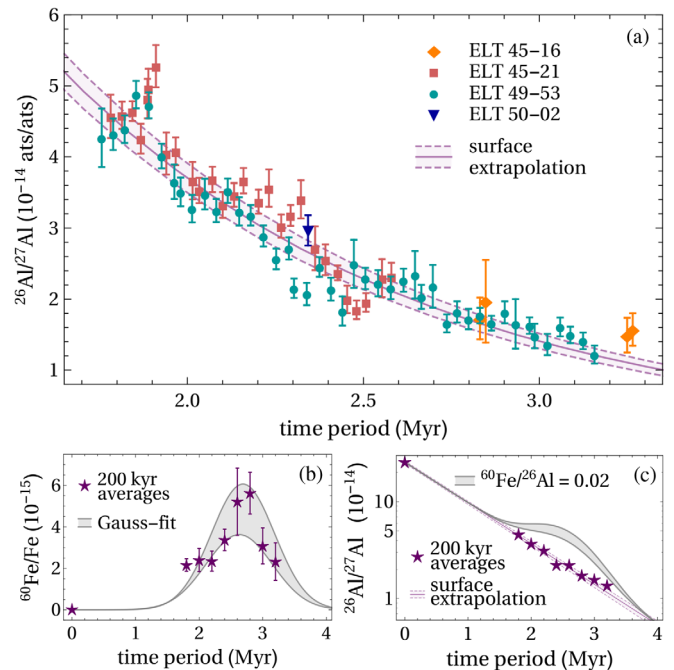FIG. 1. (a) [26]Al/[27]Al ratios of individual samples from four deep-sea sediment cores versus time, not corrected for radioactive decay. The exponential decay function derived from the measured initial (surface) ratio is displayed as a colored line with its uncertainty range. (b) Decay-corrected [60]Fe/Fe ratios as 200 kyr averages versus age, fitted with a Gaussian distribution and showing only the fit uncertainties. (c) [26]Al/[27]Al ratios as 200 kyr averages versus age, not corrected for radioactive decay (logarithmic scale). The Gaussian-shaped [60]Fe signal has been translated to SN-associated [26]Al using an isotopic ratio of [60]Fe/[26]Al = 0.02.

3.2 Myr of $(2.60 \pm 0.03) \times 10^{-13}$, suggesting a SN-associated ^{26}Al contribution was not detected. Obvious deviations from the derived exponential function, being beyond statistical fluctuations and occurring as clusters of neighbouring values that span up to about 0.2 Myr, might indicate unknown geological processes acting at these timescales. In contrast, the ^{60}Fe data indicates a SN-associated material deposition lasting more than 1 Myr [22] [Fig. 1(b)], which would be equally expected for SN-associated ^{26}Al influx. The data analysis does not show any long-term deviations from an ideal exponential decay of atmospheric ^{26}Al input; hence, we conclude that any SN-associated ^{26}Al influx is below statistical significance.

We assume that the SN-associated ^{26}Al is hidden within our ^{26}Al measurement uncertainty to derive limits in the SN-associated ^{60}Fe/^{26}Al ratio with

$$\left(\frac{^{60}\text{Fe}}{^{26}\text{Al}}\right)_{\text{SN}} \geq \frac{^{60}\text{Fe}}{\sigma(^{26}\text{Al})} = \frac{\left(\frac{^{60}\text{Fe}}{\text{Fe}}\right)_{\text{AMS}} \times \text{C}_{\text{Fe}}}{\sigma\left[\left(\frac{^{26}\text{Al}}{^{27}\text{Al}}\right)_{\text{AMS}} \times \text{C}_{^{27}\text{Al}}\right]}. \quad (1)$$

The individual ^{26}Al/^{27}Al sediment data from AMS measurements within the SN-peak interval of 1.7–3.2 Myr were converted to atom concentrations of ^{26}Al per gram using the corresponding ^{27}Al concentrations $\text{C}_{^{27}\text{Al}}$ correcting for radioactive decay. The uncertainties $\sigma(^{26}\text{Al})$ of the resulting data set increase with sediment age due to lower ^{26}Al counting statistics at higher ages [Fig. 2(a)] and pose an upper limit of SN-associated ^{26}Al influx with time. Similarly, individual ^{60}Fe/Fe data were converted to decay-corrected ^{60}Fe concentrations using the Fe concentrations C_{Fe} [Fig. 2(b), Supplementary Tables I–III].

The ratio of the SN-associated ^{60}Fe concentration to the uncertainties of the ^{26}Al concentration [Fig. 2(c)] represents a lower limit for the SN-associated ^{60}Fe/^{26}Al ratio. Note the ^{60}Fe/$\sigma(^{26}$Al) ratios are influenced by scatter in the ^{60}Fe concentrations, and the increasing uncertainty of ^{26}Al with time causes a decrease in the ratios at greater ages.

We modelled a lower limit of ^{60}Fe/^{26}Al by fitting the data using a Nadaraya-Watson kernel regression [39,40] with a confidence level of 68% [Fig. 2(c), see Supplemental Material [33]]. Calculating the mean of the function and its uncertainty in the time period of 1.5 Myr yields an average lower limit of ^{60}Fe/^{26}Al $= 0.18^{+0.15}_{-0.08}$. Hence, considering only the lower and upper bounds of the 68% uncertainty band yields two average data-derived lower limits for the SN-associated ^{60}Fe/^{26}Al ratio: a conservative minimum lower limit of ^{60}Fe/^{26}Al $\geq 0.18-0.08 = 0.10$ and a maximum lower limit of ^{60}Fe/^{26}Al $\geq 0.18+0.15 = 0.33$. For comparison, we fitted the ^{26}Al atom concentration uncertainties yielding an average upper limit of 44×10^4 atoms g^{-1} [Fig. 2(a)] and the ^{60}Fe concentration of $7.5^{+5.5}_{-3.3} \times 10^4$ atoms g^{-1} [Fig. 2(b)] to calculate the lower
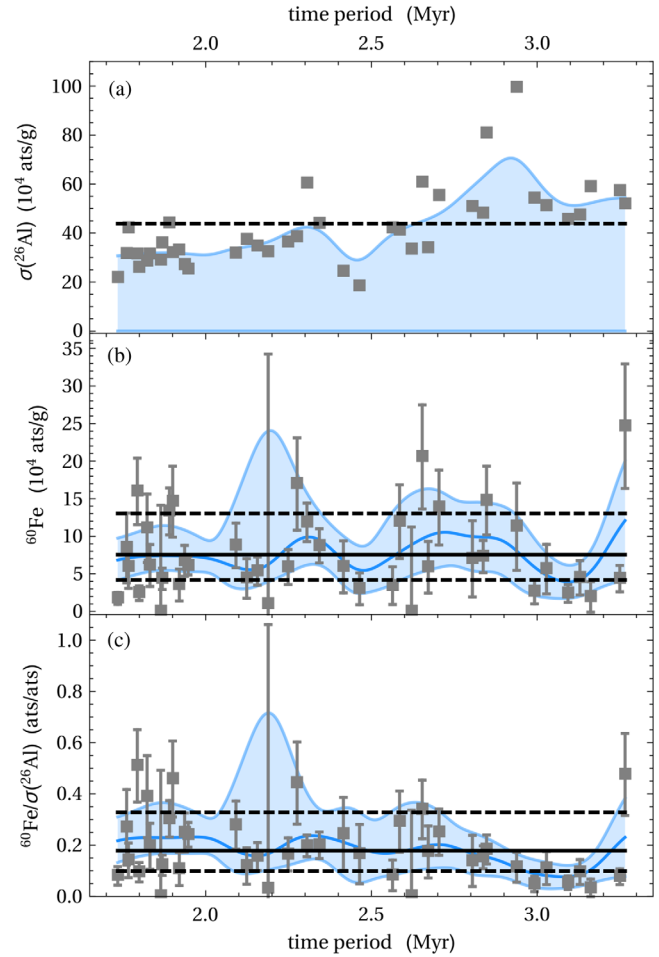

FIG. 2. ^{26}Al atom concentrations uncertainties (a) and ^{60}Fe atom concentrations (b) per gram of sediment corrected for background and radioactive decay, and their ratios (c). Panel (a) displays the regression line (solid blue) of the data as upper limit, (b) and (c) show the mean and uncertainty of each regression by solid blue lines. Their averages are displayed as solid (mean) and dashed (uncertainty) black lines.

SN-associated ^{60}Fe/^{26}Al limit yielding a similar result of $0.17^{+0.13}_{-0.08}$.

We use our derived minimum and maximum lower ^{60}Fe/^{26}Al limits in combination with the measured SN-associated ^{60}Fe data to deduce SN-associated ^{26}Al yields and check these for compatibility with our initially measured ^{26}Al/^{27}Al data. This approach requires the assumption that, after ejection by a SN, ^{60}Fe and ^{26}Al behave identically during transport and deposition on Earth. First, we modelled the measured and decay-corrected ^{60}Fe/Fe time profile with a Gaussian fit of the data, yielding a signal centered at 2.64 Myr with a full width at half maximum of 1.14 Myr [Fig. 1(b)]. Next, we converted this signal to the absolute amount of ^{60}Fe using concentrations of stable Fe $(1.81 \pm 0.03 \times 10^{19}$ atoms g^{-1} on average, see Supplemental Material [33]). Subsequently, we calculated the corresponding amount of ^{26}Al, which we translated to a ^{26}Al/^{27}Al time
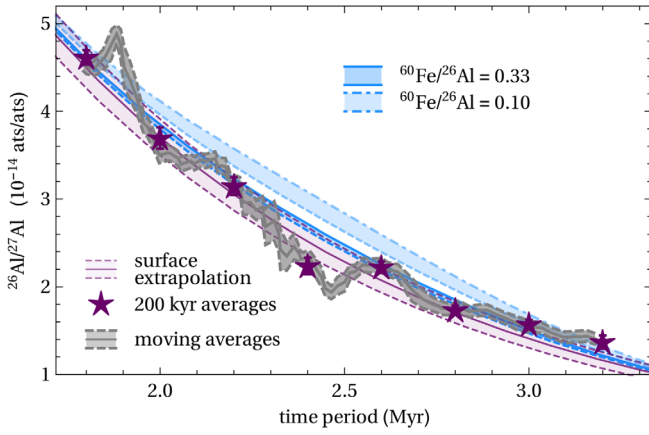
FIG. 3.   200 kyr-averages of ^{26}Al/^{27}Al isotope ratios, a moving average summed over five adjacent data points and the exponential function derived from modern samples versus sediment age. The two SN-associated ^{26}Al signals on top of atmospheric input (blue) correspond to the specific lower ^{60}Fe/^{26}Al limits derived from experimental data.

profile using the measured average concentration of stable ^{27}Al ($1.86 \pm 0.07 \times 10^{19}$ atoms g^{-1}). Taking the exponential decay into account, we added the ^{26}Al/^{27}Al time profile to the exponential function obtained from the modern surface samples (Fig. 3). The maximum lower SN-associated ^{26}Al/^{60}Fe limit of 0.33 results in a SN-associated ^{26}Al signal hidden within the uncertainty of the terrestrial influx. A higher ^{26}Al SN influx, based on the minimum lower limit of 0.10, indicates a SN signal that is not entirely supported by the 200 kyr and moving averages of the measured ^{26}Al/^{27}Al data.

In the following, we examine the wide range of reported ^{60}Fe/^{26}Al ratios deduced from stellar nucleosynthesis models for compatibility with our experimental data. Different input physics (e.g., reaction rates, stellar rotation) in the nucleosynthesis models leads to ^{60}Fe/^{26}Al production ratios for SNe that vary between 0.02 and 2 over the stellar initial mass range of $9 - 25$ $M_\odot$ [11–13,41–44].

As an example, we use the lowest reported ^{60}Fe/^{26}Al ratio of 0.02 [13] to convert the Gaussian-shaped ^{60}Fe time profile [Fig. 1(b)] to a SN-associated ^{26}Al/^{27}Al time profile, which is added to the exponential function obtained from modern surface samples. The resulting signal from the model is not observed in the measured data [Fig. 1(c)], but shows that ^{26}Al would have been detected if the SN ejecta reaching Earth would have carried this low ^{60}Fe/^{26}Al ratio.

Thus, our experimental SN-associated ^{60}Fe/^{26}Al limits are in agreement with most of the CCSN-associated ratios derived from stellar nucleosynthesis calculations (Fig. 4). ECSNe (not included in Fig. 4) are proposed to have a high ^{60}Fe yield but negligible ^{26}Al production during explosive nucleosynthesis. After exploding, the expanding remnant of the ECSN picks up the matter blown out by the stellar winds of its prior SAGB phase [45] that contains large
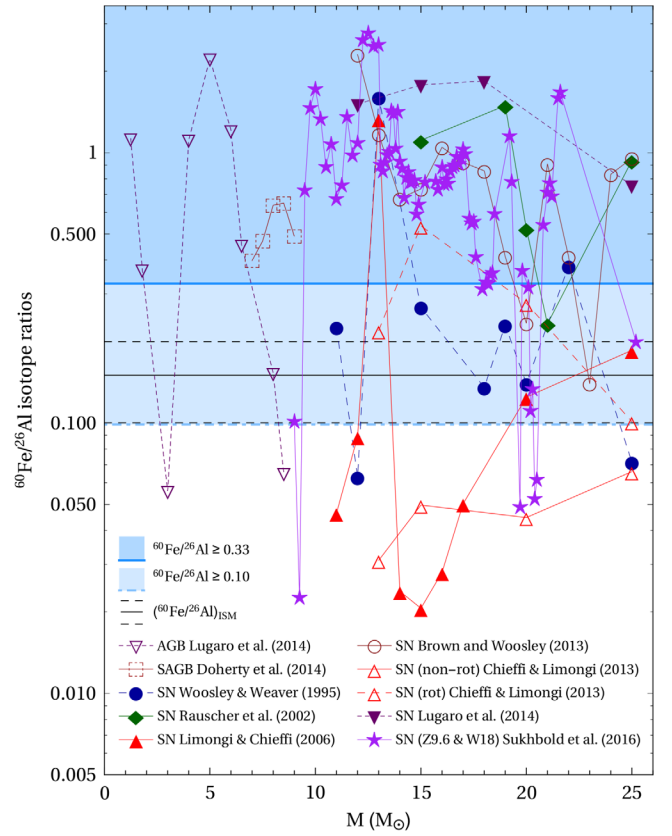

FIG. 4. ^{60}Fe/^{26}Al nucleosynthesis isotope ratios [10–13,41–44] versus initial stellar mass. We display ratios of (S)AGB stars and SNe that contribute ^{26}Al and ^{60}Fe to the ISM as well as the galactic average γ-flux ratio. The shaded blue areas indicate the possible SN-associated ^{60}Fe/^{26}Al ratios derived from our measured ^{26}Al data. Abbreviations denote rotating (rot) and nonrotating (non-rot) stellar models [43]. Z9.6 and W18 refer to pre-SN evolution models in the mass ranges of $9 - 12$ $M_\odot$ and $12.5 - 25.2$ $M_\odot$, respectively [44].

amounts of ^{26}Al and ^{60}Fe ([10], Fig. 4). In such a scenario, the total ^{26}Al/^{60}Fe isotope ratio becomes

$$\left(\frac{^{60}\text{Fe}}{^{26}\text{Al}}\right)_{\text{final}} = \frac{^{60}\text{Fe}_{\text{SAGB}} + {}^{60}\text{Fe}_{\text{ECSN}}}{^{26}\text{Al}_{\text{SAGB}}} \times \frac{26}{60}. \qquad (2)$$

For example, the lowest modelled ^{60}Fe/^{26}Al SAGB isotopic ratio from Doherty *et al.* [10] is 0.39 (a 7 $M_\odot$ star, Fig. 4), derived from the SAGB yields of 2.817×10^{-6} $M_\odot$ of ^{60}Fe and 3.064×10^{-6} $M_\odot$ of ^{26}Al. If this star explodes as ECSN, an additional ^{60}Fe SN contribution, with a yield ranging from 3.61×10^{-5} $M_\odot$ to 1.3×10^{-4} $M_\odot$ [14], may increase the original ^{60}Fe/^{26}Al SAGB ratio to 5.5–18.8. Our results agree with previous studies that suggested ECSNe as primary candidates for the origin of the ^{60}Fe signal 2–3 Myr ago [46,47]. However, our sediment data is also consistent with nucleosynthesis models for more massive stars.

The modelled SN-associated ^{60}Fe/^{26}Al nucleosynthesis ratios are usually integrated over the IMF (initial mass function, mass distribution of stars in a stellar cluster at birth) to obtain an average galactic steady-state ratio. This ratio is, for some SN nucleosynthesis models, higher than the ^{60}Fe/^{26}Al γ-flux ratio observed in the ISM of (0.15 ± 0.05) [8,12,41,44]. It has been suggested that this difference could be bridged by additional sources, such as the stellar winds of WR stars that add a significant fraction of ^{26}Al to the ISM [16,48]. Our experimental lower limits for ^{60}Fe/^{26}Al map recent specific local SN events within our solar environment, as opposed to the steady-state conditions of the ISM. Since our data set provides lower limits, it does not exclude, for example, an additional WR source enriching the galactic mixture with ^{26}Al and thus lowering the observed γ-flux ratio compared to the SN-associated ^{60}Fe/^{26}Al ratios.

We note, that all statements made so far assume that ^{60}Fe and ^{26}Al are transported equally to the Solar System within dust particles. It is in fact not clear whether their isotopic ratio is conserved during the journey, e.g., due to different dust survival rates within the SN remnant [47,49] and nonisotropic clumpy ejecta [50]. However, the ^{60}Fe signal is advocated to originate from a series of nearby SN explosions forming the local superbubble in which our Solar System is embedded [24,46,51]. The combined ejecta from a number of SNe could average out some of the inhomogeneities between ^{26}Al and ^{60}Fe.

Under the assumptions made, we can conclude that the astrophysical scenarios proposed to explain the SN-associated ^{60}Fe signal (ECSNe, CCSNe) are consistent with our results derived from ^{26}Al measurements. The nondetection of ^{26}Al provides a constraint on the SN-associated ^{60}Fe/^{26}Al isotope ratio in the solar environment in the recent past.

[*]feige@astro.physik.tu-berlin.de

[1] M. S. Basunia and A. M. Hurst, Nucl. Data Sheets **134,** 1 (2016).

[2] G. Rugel, T. Faestermann, K. Knie, G. Korschinek, M. Poutivtsev, D. Schumann, N. Kivel, I. Günther-Leopold, R. Weinreich, and M. Wohlmuther, Phys. Rev. Lett. **103,** 072502 (2009).

[3] A. Wallner, M. Bichler, K. Buczak, R. Dressler, L. K. Fifield, D. Schumann, J. H. Sterba, S. G. Tims, G. Wallner, and W. Kutschera, Phys. Rev. Lett. **114,** 041101 (2015).

[4] K. M. Ostdiek, T. S. Anderson, W. K. Bauder, M. R. Bowers, A. M. Clark, P. Collon, W. Lu, A. D. Nelson, D. Robertson, M. Skulski, R. Dressler, D. Schumann, J. P. Greene, W. Kutschera, and M. Paul, Phys. Rev. C **95,** 055809 (2017).

[5] E. Zinner, S. Amari, E. Anders, and R. Lewis, Nature (London) **349,** 51 (1991).

[6] A. Shukolyukov and G. W. Lugmair, Earth Planet. Sci. Lett. **119,** 159 (1993).

[7] R. Diehl, M. Lang, K. Kretschmer, and W. Wang, New Astron. Rev. **52,** 440 (2008).

[8] W. Wang, in *The Art of Modeling Stars in the 21st Century, Proceedings of the International Astronomical Union, IAU Symposium,* edited by L. Deng and K. L. Chan (2008), Vol. 252, pp. 333–338, http://adsabs.harvard.edu/abs/2008IAUS..252..333W.

[9] M. Lugaro and A. I. Karakas, New Astron. Rev. **52,** 416 (2008).

[10] C. L. Doherty, P. Gil-Pons, H. H. B. Lau, J. C. Lattanzio, and L. Siess, Mon. Not. R. Astron. Soc. **437,** 195 (2014).

[11] S. E. Woosley and T. A. Weaver, Astrophys. J. Suppl. Ser. **101,** 181 (1995).

[12] T. Rauscher, A. Heger, R. D. Hoffman, and S. E. Woosley, Astrophys. J. **576,** 323 (2002).

[13] M. Limongi and A. Chieffi, Astrophys. J. **647,** 483 (2006).

[14] S. Wanajo, H.-T. Janka, and B. Müller, Astrophys. J. Lett. **774,** L6 (2013).

[15] N. Prantzos and R. Diehl, Phys. Rep. **267,** 1 (1996).

[16] A. Palacios, G. Meynet, C. Vuissoz, J. Knödlseder, D. Schaerer, M. Cerviño, and N. Mowlavi, Astron. Astrophys. **429,** 613 (2005).

[17] V. V. Dwarkadas, N. Dauphas, B. Meyer, P. Boyajian, and M. Bojazi, Astrophys. J. **851,** 147 (2017).

[18] G. Korschinek, T. Faestermann, K. Knie, and C. Schmidt, Radiocarbon **38,** 68 (1996).

[19] J. Ellis, B. D. Fields, and D. N. Schramm, Astrophys. J. **470,** 1227 (1996).

[20] K. Knie, G. Korschinek, T. Faestermann, C. Wallner, J. Scholten, and W. Hillebrandt, Phys. Rev. Lett. **83,** 18 (1999).

[21] K. Knie, G. Korschinek, T. Faestermann, E. A. Dorfi, G. Rugel, and A. Wallner, Phys. Rev. Lett. **93,** 171103 (2004).

[22] A. Wallner, J. Feige, N. Kinoshita, M. Paul, L. K. Fifield, R. Golser, M. Honda, U. Linnemann, H. Matsuzaki, S. Merchel, G. Rugel, S. G. Tims, P. Steier, T. Yamagata, and S. R. Winkler, Nature (London) **532,** 69 (2016).

[23] P. Ludwig, S. Bishop, R. Egli, V. Chernenko, B. Deneva, T. Faestermann, T. Famulok, L. Fimiani, L. J. M. Gómez-Guzmán, K. Hain, G. Korschinek, M. Hanzlik, S. Merchel, and G. Rugel, Proc. Natl. Acad. Sci. U.S.A. **113,** 9232 (2016).

[24] J. Feige, D. Breitschwerdt, A. Wallner, M. M. Schulreich, N. Kinoshita, M. Paul, C. Dettbarn, L. K. Fifield, R. Golser, M. Honda, U. Linnemann, H. Matsuzaki, S. Merchel, G. Rugel, P. Steier, S. G. Tims, S. R. Winkler, and T. Yamagata, in *Proceedings of the 14th International Symposium on Nuclei*

in the Cosmos (NIC2016), edited by S. Kubono, T. Kajino, S. Nishimura, T. Isobe, S. Nagataki, T. Shima, and Y. Takeda (2017), p. 010304, http://adsabs.harvard.edu/abs/2017nuco.confa0304F.

[25] L. Fimiani, D. L. Cook, T. Faestermann, J. M. Gómez-Guzmán, K. Hain, G. Herzog, K. Knie, G. Korschinek, P. Ludwig, J. Park, R. C. Reedy, and G. Rugel, Phys. Rev. Lett. **116,** 151104 (2016).

[26] L. A. Frakes, Sedimentology Res. Lab. Contrib. **33,** 105 (1971).

[27] L. A. Frakes, Sedimentology Res. Lab. Contrib. **37,** 259 (1973).

[28] J. Feige, A. Wallner, L. K. Fifield, G. Korschinek, S. Merchel, G. Rugel, P. Steier, S. R. Winkler, and R. Golser, EPJ Web Conf. **63,** 03003 (2013).

[29] E. Allison and M. T. Ledbetter, Mar. Geol. **46,** 131 (1982).

[30] D. Bourlès, G. M. Raisbeck, and F. Yiou, Geochim. Cosmochim. Acta **53,** 443 (1989).

[31] S. Merchel and U. Herpers, Radiochim. Acta **84,** 215 (1999).

[32] G. J. Wasserburg, R. Gallino, and M. Busso, Astrophys. J. Lett. **500,** L189 (1998).

[33] See Supplemental Material http://link.aps.org/supplemental/10.1103/PhysRevLett.121.221103, which contains data tables and description of data fitting.

[34] M. Auer, W. Kutschera, A. Priller, D. Wagenbach, A. Wallner, and E. M. Wild, Nucl. Instrum. Methods Phys. Res., Sect. B **259,** 595 (2007).

[35] D. Lal and B. Peters, Handbuch Phys. **46,** 551 (1967).

[36] M. Auer, D. Wagenbach, E. M. Wild, A. Wallner, A. Priller, H. Miller, C. Schlosser, and W. Kutschera, Earth Planet. Sci. Lett. **287,** 453 (2009).

[37] K. J. Orians and K. W. Bruland, Earth Planet. Sci. Lett. **78,** 397 (1986).

[38] P. Sharma and R. Middleton, Geochim. Cosmochim. Acta **53,** 709 (1989).

[39] E. A. Nadaraya, Theory Probab. Appl. **9,** 141 (1964).

[40] G. S. Watson, Indian J. Stat. **26,** 359 (1964).

[41] M. Lugaro, A. Heger, D. Osrin, S. Goriely, K. Zuber, A. I. Karakas, B. K. Gibson, C. L. Doherty, J. C. Lattanzio, and U. Ott, Science **345,** 650 (2014).

[42] J. M. Brown and S. E. Woosley, Astrophys. J. **769,** 99 (2013).

[43] A. Chieffi and M. Limongi, Astrophys. J. **764,** 21 (2013).

[44] T. Sukhbold, T. Ertl, S. E. Woosley, J. M. Brown, and H.-T. Janka, Astrophys. J. **821,** 38 (2016).

[45] T. J. Moriya, N. Tominaga, N. Langer, K. Nomoto, S. I. Blinnikov, and E. I. Sorokina, Astron. Astrophys. **569,** A57 (2014).

[46] D. Breitschwerdt, J. Feige, M. M. Schulreich, M. A. D. Avillez, C. Dettbarn, and B. Fuchs, Nature (London) **532,** 73 (2016).

[47] B. J. Fry, B. D. Fields, and J. R. Ellis, Astrophys. J. **800,** 71 (2015).

[48] N. Prantzos, Astron. Astrophys. **420,** 1033 (2004).

[49] B. J. Fry, B. D. Fields, and J. R. Ellis, Astrophys. J. **827,** 48 (2016).

[50] C. Biscaro and I. Cherchneff, Astron. Astrophys. **564,** A25 (2014).

[51] M. M. Schulreich, D. Breitschwerdt, J. Feige, and C. Dettbarn, Astron. Astrophys. **604,** A81 (2017).